Satellite Products and Services Review Board

Enterprise Land Surface Emissivity Algorithm Theoretical Basis Document

Compiled by the

Land Surface Temperature Algorithm Working Group

Version 1.2

March, 2018

TITLE: ENTERPRISE LAND SURFACE EMISSIVITY ALGORITHM THEORETICAL BASIS DOCUMENT

AUTHORS:

Yunyue Yu, NOAA/NESDIS/STAR, College Park, MD

Heshun Wang, UMD/CICS, College Park, MD

Yuling Liu, UMD/CICS, College Park, MD

Peng Yu, UMD/CICS, College Park, MD

DOCUMENT HISTORY
DOCUMENT REVISION LOG

The Document Revision Log identifies the series of revisions to this document since the baseline release. Please refer to the above page for version number information.

DOCUMENT TITLE: Enterprise Land Surface Emissivity Algorithm Theoretical Basis Document			
DOCUMENT CHANGE HISTORY			
Revision No.	**Date**	**Revision Originator Project Group**	**CCR Approval # and Date**
1.0	June 2016	Initial create by Heshun Wang	
1.1	September 2017	Revised by LST algorithm working group (Yunyue Yu, Heshun Wang, Peng Yu and Yuling Liu)	
1.2	March 2018	Revised by LST algorithm working group	

LIST OF CHANGES

Significant alterations made to this document are annotated in the List of Changes table.

DOCUMENT TITLE: Enterprise Land Surface Emissivity Algorithm Theoretical Basis Document					
LIST OF CHANGE-AFFECTED PAGES/SECTIONS/APPENDICES					
Version Number	**Date**	**Changed By**	**Page**	**Section**	**Description of Change(s)**
1.1	10/16/2017	HeshunWang	14-21	2.3	Update algorithm descriptions
1.2	03/28/2018	HeshunWang	25	2.6.4	Update exception handling section

TABLE OF CONTENTS

LIST OF TABLES AND FIGURES

1 INTRODUCTION

In this section, the background and requirement of the land surface emissivity (LSE) product will be introduced along with satellite instrument descriptions. Section 2 provides detailed description of the LSE retrieval algorithm and operations concept including the algorithm theoretical basis, processing outline, input/output data, error budget and practical considerations during the operation. Finally, validation strategies and preliminary results are provided. Assumptions and limitations associated with the algorithm are discussed in Section 3. Finally, Section 4 lists the references cited.

1.1 Product Overview

1.1.1 Product Description

Land surface temperature (LST) as an important proxy of surface energy is required in a wide variety of applications of hydrology, meteorology and climatology (Wan and Dozier 1996, Yu et al. 2005). Remote sensing is a unique approach which allows global and regional coverage for LST. Many algorithms have been proposed to retrieve LST from thermal infrared (TIR) observations (Dash et al. 2002, Li et al. 2013), in which temperature coupled with LSE and atmospheric downward radiance. From the perspective of emissivity, these methods could be roughly classified into two types: LST retrieval with known LSE, such as split window (SW) algorithm and single-channel algorithm (Wan and Dozier 1996, Jiménez-Muñoz 2003), and simultaneous temperature and emissivity separation (Wan and Li 1997, Gillespie et al. 1998). The latter one requires more temporal or spectral information. For sensors with only one or two TIR channels, emissivity is an important input and its variation is still the biggest impediment in satellite LST retrieval (Becker 1987, Qin et al. 2001, Yu et al. 2008). Besides, as an intrinsic property of the surface, broad band emissivity is important for the precise determination of longwave radiative energy, and this is particularly necessary for arid/semi-arid regions, where LSE deviate considerably from the behavior of black body. Satellite LST&E have been assimilated into climate, atmospheric and land surface models and high quality LSE has demonstrated its significant contribution (Jin and Liang 2006, Vogel et al. 2011).

The Joint Polar Satellite System (JPSS) and the Geostationary Operational Environmental Satellites R Series (GOES-R) are the nation’s next generation of the polar-orbiting environmental satellites and geostationary weather satellites, respectively. The Visible Infrared Radiometer Suite (VIIRS) onboard JPSS series and the Advanced Baseline Imager (ABI) onboard GOES-R will play an important role in developing LST records. The new proposed LSE product will enhance LST production of JPSS and GOES-R missions as well

as to support forecasting models. In the United States of America, demands of satellite LSE data are from a variety of government agencies as well as from universities and research institutes.

1.1.2 Product Requirements

LSE product is primarily designed to support LST product to meet the requirement of LST accuracy. We define LSE product requirement according to current algorithm performance and input data quality. The individual requirements for each satellite missions along with the broad band are listed in Table 1-1.

Table 1-1 LSE Product Requirement

	VIIRS	ABI	Broadband
Spatial Coverage	Global Gridded	Global Gridded	Global Gridded
Spectral Coverage	M15(10.26–11.26 μm) M16(11.54–12.49 μm)	Ch14(10.8-11.6 μm) Ch15(11.8-12.8 μm)	8-13.5 μm
LSE Accuracy	0.01	0.01	0.015
LSE Precision	0.015	0.015	0.02
Data Range	0-1	0-1	0-1
Refresh Rate	Daily	Daily	Daily
Horizontal resolution	0.009×0.009 degree	0.009×0.009 degree	0.009×0.009 degree
Mapping Uncertainty	3 sigma of 1km	3 sigma of 1km	3 sigma of 1km

1.2 Satellite Instrument Description

VIIRS onboard S-NPP and future JPSS series satellites collect visible and infrared imagery and radiometric measurements of the land, atmosphere, cryosphere, and oceans. It is a new generation of operational moderate resolution-imaging instrument following the legacy from the Advanced Very High Resolution Radiometer (AVHRR) on NOAA family of polar orbiting platforms and the Moderate Resolution Imaging Spectroradiometer (MODIS) on Terra and Aqua satellites. Based on VIIRS data, many critical environmental products are generated, including snow and ice cover, clouds and aerosols properties, ocean color, sea and land surface temperature, vegetation health and surface albedo. These variables greatly benefit the operational weather community towards a more precise prediction of weather, flooding, and storm, etc.

VIIRS provides global moderate-resolution data twice a day without any gap. It is a scanning radiometer with a total field of view of 112.56° in the cross-track direction. The swath width is about 3060 km at a nominal equatorial altitude of 829 km, providing full global daily coverage in both daytime and nighttime. Its 22 spectral bands, from 0.4 to 12.5μm (Table 1-2), provide data for the production of more than 20 Environmental Data Records (EDRs).

There are 16 moderate-resolution bands (M bands, each with 16 detectors) with a spatial resolution of 750m at nadir, five imaging resolution bands (I bands, each with 32 detectors) with a 375m spatial resolution at nadir, and one panchromatic DNB with a near constant 750m spatial resolution throughout the scan. The M bands include 11 reflective solar bands (RSB) and 5 thermal emissive bands (TEB) which includes the two split window channels used for LST retrieval, and the I bands include 3 RSB and 2 TEB(Cao et al., 2013). Detailed spectral characteristics are summarized in Table 1-2.

Table 1-2 Spectral Characteristics of VIIRS

		Bands NO.	Driving EDR(s)	Spectral Range(μm)	Resolution(m)
Reflective Bands	VIS/NIR	M1	Ocean Color, Aerosol	0.402-0.422	750
		M2	Ocean Color, Aerosol	0.436-0.454	750
		M3	Ocean Color, Aerosol	0.478-0.488	750
		M4	Ocean Color, Aerosol	0.545-0.565	750
		I1	Imagery EDR	0.600-0.680	375
		M5	Ocean Color, Aerosol	0.662-0.682	750
		M6	Atmospheric Correction	0.739-0.754	750
		I2	NDVI	0.850-0.880	375
		M7	Ocean Color, Aerosol	0.846-0.885	750
		DNB	Day & Night	0.500-0.900	750
	S/MWIR	M8	Cloud Particle Size	1.230-1.250	750
		M9	Cirrus/Cloud Cover	1.371-1.386	750
		I3	Binary Snow Map	1.580-1.640	375
		M10	Snow Fraction	1.580-1.640	750
		M11	Clouds	2.230-2.280	750
Emissive Bands		I4	Imagery Clouds	10.26-11.26	375
		M12	SST	3.610-3.790	750
		M13	SST, Fire	3.970-4.130	750
	LWIR	M14	Cloud Top Properties	8.400-8.700	750
		M15	**LST**	**11.54-12.49**	**750**
		I5	Imagery Cloud	10.50-12.40	375
		M16	**LST**	**11.54-12.49**	**750**

ABI is the primary instrument on the GOES-R Series observing the earth's weather, oceans, and environment. It is a multi-channel passive imaging radiometer designed to observe the western hemisphere with multiple spatial domains. The instrument has two scan modes; the default mode concurrently takes a full disk (FD) image every 15 minutes, a Continental U.S. (CONUS) image every five minutes, and two meso-scale images every 60 seconds. ABI can

also operate in continuous FD mode, providing uninterrupted FD scans every 5 minutes. ABI views the Earth with 16 different spectral bands, including two visible channels, four near-infrared channels, and ten infrared channels. Its spatial resolution is nominally 2 km for the infrared bands and 0.5 km for the 0.64μm visible band (Schmit et al., 2007). More details are provided in Table 1-3.

ABI is used in a wide range of applications related to weather, oceans, land, climate and hazards (fires, volcanoes, floods, hurricanes and storms that spawn tornadoes). It tracks and monitors cloud information, atmospheric motion, convection, land surface temperature, ocean dynamics, flow of water, fire, smoke, volcanic ash plumes, aerosols and air quality, and vegetative health. ABI's data enables meteorologists to pinpoint and track developing storms in much greater detail. Benefits from the ABI include improved tropical cyclone forecasts, fewer weather-related flight delays and airline incidences with volcanic plumes, improved production and distribution of electricity and natural gas, increased efficiency in irrigated water usage in agriculture, and higher protection rates for recreational boats in the event of a tropical storm or hurricane.

Table 1-3 Spectral Characteristics of ABI

Channel Number	Wavelength (μm)	Bandwidth(μm)	NEDT/SNR	Spatial Resolution
1	0.47	0.45 – 0.49	300:1[1]	1 km
2	0.64	0.59 – 0.69	300:1[1]	0.5 km
3	0.86	0.8455 – 0.8845	300:1[1]	1 km
4	1.38	1.3705 – 1.3855	300:1[1]	2 km
5	1.61	1.58 – 1.64	300:1[1]	1 km
6	2.26	2.225 – 2.275	300:1[1]	2 km
7	3.9	3.8 – 4.0	0.1K[2]	2 km
8	6.15	5.77 – 6.60	0.1K[2]	2 km
9	7.0	6.75 – 7.15	0.1K[2]	2 km
10	7.4	7.24 – 7.44	0.1K[2]	2 km
11	8.5	8.30 – 8.70	0.1K[2]	2 km
12	9.7	9.42 – 9.80	0.1K[2]	2 km
13	10.35	10.10 – 10.60	0.1K[2]	2 km
14	11.2	10.80 – 11.60	0.1K[2]	2 km
15	12.3	11.80 – 12.80	0.1K[2]	2 km
16	13.3	13.0 – 13.6	0.3K[2]	2 km

[1]100% albedo, [2]300Kscene.Shaded channels are used for LST retrieval.

2 ALGORITHM DESCRIPTION

2.1 Processing Outline

LSE product is generated based on the vegetation cover method (VCM), which combines two constant emissivity values from the bare ground and full vegetation situations of each pixel. The real time emissivity is adjusted according to the green vegetation fraction (GVF). The processing includes two parts as figure 2-1 shows: the static emissivity module aims to generate background component. Emissivity climatology served as the bare component in the algorithm, and the dynamic emissivity module accounts for the emissivity variation due to GVF and snow fraction.

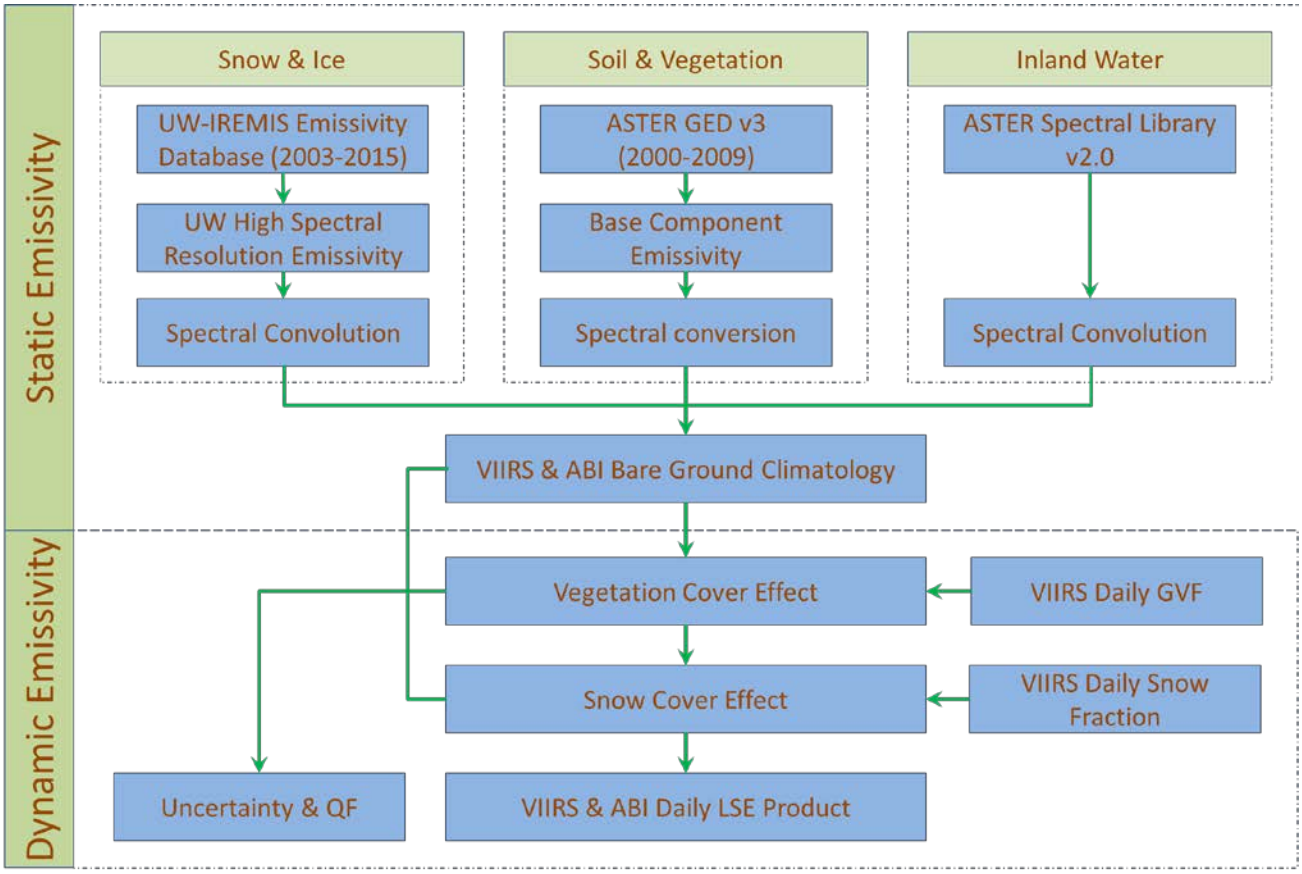

Figure 2-1 LSE algorithm description

In the static emissivity module, land surface is classified into three types with different processing approaches according to their thermal emission characteristics. The permanent snow & ice emissivities are directly converted from the mean value of a long term MODIS

emissivity product; the values of the inland water are determined according to Advanced Space borne Thermal Emission and Reflection Radiometer (ASTER) spectral library dataset, and those of soil and vegetation area, also the most common situations, are derived using ASTER Global Emissivity Dataset (GED) dataset and related mean normalized difference vegetation index (NDVI) using the reverse form of the VCM. More details are given in the section 2.3.

VIIRS/ABI bare ground emissivity climatology, VIIRS GVF and snow fraction are used in the dynamic emissivity module to derive the daily emissivity and its associated quality flags to determine the data quality. The dynamic LSE processing flowchart is demonstrated in Figure 2-2.

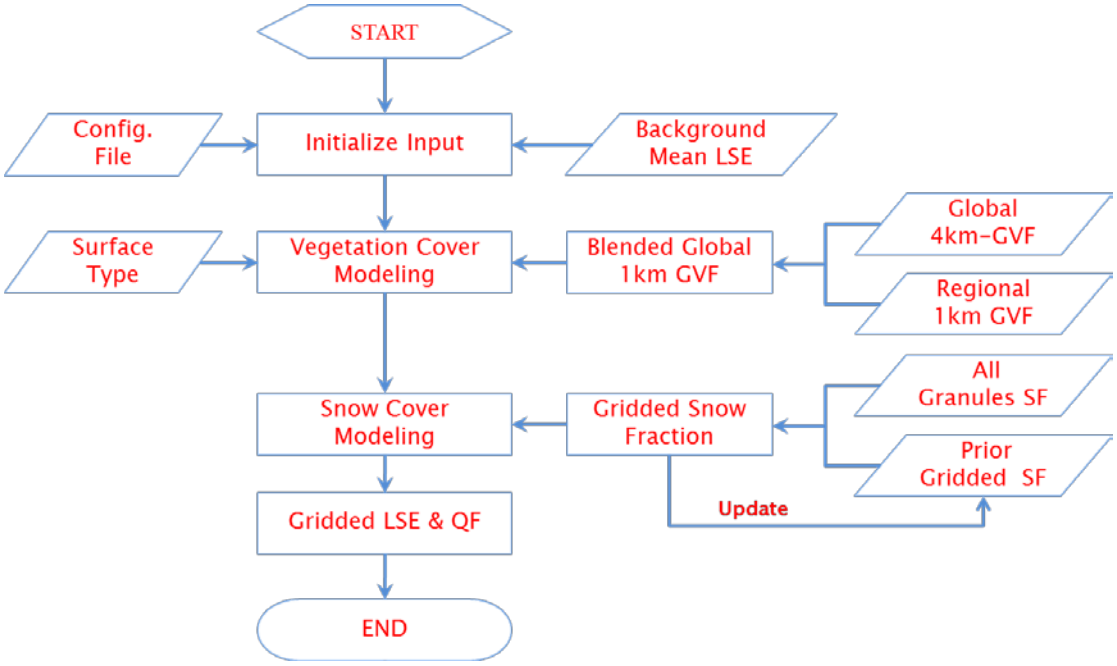

Figure 2-2 LSE Processing Flowchart

2.2 Algorithm Input

This section describes the input needed to process the LSE product. Both the VIIRS and ABI LSE use VIIRS EDR product as primary input to account for the dynamic change. Apart from the satellite product, LSE algorithm requires the ancillary data such as bare ground emissivity and the look-up table, in which VIIRS and ABI have their own input data designed for certain channel.

2.2.1 Derived sensor data

There are three types of derived data from VIIRS: VIIRS GVF, VIIRS annual surface type and VIIRS snow fraction.
Currently, VIIRS GVF provides data in two different spatial resolutions: global coverage at 4km resolution and North America coverage (130°E to 30°E, 90°N to 7.5°S) at 1km grids. They will be employed to generate a global GVF at 0.009 degree with degraded value apart from the North America region.
VIIRS Global Surface Type (GST) is also taken as an input for emissivity calculation. Updated annually, GST is generated with the 17-type classification scheme of the International Geosphere-Biosphere Program (IGBP) and is produced at a 1-kilometer spatial resolution.
VIIRS reflectance based snow fraction is another important input for LSE product. All the granules of prior day are used to update the snow information for the near-real-time dynamic emissivity. Table 2-1lists the primary derived sensor data used in the LSE algorithm.

Table 2-1 LSE product algorithm input

Name	Type	Source	Description	Dimension
VIIRS gridded GVF	Dynamic	NDE	VIIRS 4km global weekly GVF	grid (xsize, ysize)1
	Dynamic	NDE	VIIRS weekly 1km GVF for North America	grid (xsize, ysize)2
Surface Type	Static	DAP	VIIRS Global Surface Type	grid (xsize, ysize)3
VIIRS Snow Fraction	Dynamic	NDE	VIIRS reflectance based snow fraction	granule (xsize, ysize)

NDE: S-NPP Data Exploration, DAP: Delivery Algorithm Package
1. xsize = 10000, ysize = 5000; 2. xsize = 28889, ysize = 10833; 3. xsize = 40000, ysize = 20000

2.2.2 Ancillary data

The background emissivity will serve as ancillary data along with the previous day's gap free snow fraction. For VIIRS LSE, background emissivity contains emissivity and uncertainty of three bands (VIIRS M15, M16 and broadband), plus the background surface type, and for ABI background emissivity, there are only two narrow channels (ABI ch14 and ch15).
LSE is a global product without any gap over land surface, however, the snow fraction data has filled value due to the cloud or darkness, a gap free snow fraction with latest available snow information is provided here to replace these areas.
To handle the possible exception, GVF and snow fraction monthly climatology are provided as ancillary data, once there are expected input data for LSE calculation, the climatology data will be adopted.
The following table lists and briefly describes the ancillary data required to generate the LSE.

Table 2-2 LSE product algorithm ancillary input

Name	Type	Source	Description	Dimension
VIIRS Background Emissivity Climatology	Static	DAP	Table containing predefined emissivity, uncertainty and surface type	7 variables; each of grid (xsize, ysize)[1]
ABI Background Emissivity Climatology	Static	DAP	Table containing predefined emissivity, uncertainty and surface type	5 variables; each of grid (xsize, ysize)[1]
Gap free Snow Fraction	Dynamic	DAP	Prior gap-free gridded snow fraction	grid (xsize, ysize)[1]
GVF monthly climatology	Static	DAP	VIIRS monthly mean GVF from 2013 to 2017	grid (xsize, ysize)[1]
Snow fraction monthly climatology	Static	DAP	VIIRS monthly mean Snow fraction from 2014 to 2017	grid (xsize, ysize)[1]

1. xsize = 40000, ysize = 20000;

2.2.3 Look-up tables

In addition to the derived sensor data and the ancillary data, algorithm also requires some look-up tables for algorithm implementation and control. This includes vegetation emissivity (4 narrow channels and 1 broadband) and correction factors for each surface type (17 IGBP classes), snow emissivity and uncertainty at VIIRS/ABI SW channels.

2.3 Theoretical Description

2.3.1 Physical Description

Both VIIRS and ABI have the split window channels centered at around 11μm and 12μm for LST retrieval (Table 1-2 and 1-3). To support LST retrievals for the two missions, LSE product includes four narrow bands emissivity: VIIRS M15 & M16and ABI B14 &B15and a thermal broadband emissivity which will be used for LST validation and the surface models. LSE product is generated based on the vegetation cover method, in which each pixel assumedly consists of the vegetation and bare ground components. A linear model is adopted to estimate pixel emissivity using the vegetation components proportion. In order to account for the interaction at the structured and rough surface, a compensation factor, named cavity term derived from the geometric model (Caselles and Sobrino 1989), was considered. The effective pixel level emissivity ε_λ could be calculated by:

$$\varepsilon_\lambda = \varepsilon_\lambda^{bare}\left(1-f\right)+\varepsilon_\lambda^{veg} f + d\varepsilon_\lambda \quad (2\text{-}1)$$

where $\varepsilon_{\lambda}^{bare}$ and $\varepsilon_{\lambda}^{veg}$ are the emissivity values of the bare component and vegetation at wavelength of λ, respectively, f is the fraction of vegetation cover and $d\varepsilon_{\lambda}$ is the cavity term.

In traditional VCM algorithm, both the bare and vegetation component emissivity of each surface type were assigned according to the spectral library data, which works well for the vegetation part with high and stable emissivity. However, soil emissivity could vary from as low as 0.6 to nearly 1 in TIR bands due to the diverse mineral components, soil moisture content, and surface roughness. A simple constant value from the limited spectrum in the spectral library might introduce large uncertainty especially for the arid area with spare vegetation coverage. A high spatial resolution bare component emissivity map with more detailed information is needed to fix this issue. Historical emissivity products, such as ASTER and MODIS, were employed to generate this bare emissivity climatology for this purpose. It should be noted that a conversion between narrow channel emissivities is required from source sensors to target ones.

To account for the seasonal variation, the dynamic surface parameters closely related to the emissivity are introduced to adjust the bare emissivity climatology. In the concept of VCM, the phenology is the predominant factor in the land cover change in most areas so that the real time fractional vegetation cover is indispensable to produce dynamic emissivity.

Snow with distinct emissivity spectral characters is a common natural phenomenon in the middle and high latitude regions during winter time. The snowfall can dramatically change the LSE and should not be neglected. To improve the data quality, a simple linear model was adopted for the snow effect.

$$\varepsilon_{\lambda} = \varepsilon_{\lambda}^{bv}\left(1 - f_{SF}\right) + \varepsilon_{\lambda}^{snow} f_{SF} \qquad (2\text{-}2)$$

where, $\varepsilon_{\lambda}^{bv}$ is the emissivity after the vegetation adjustment, $\varepsilon_{\lambda}^{snow}$ is snow component emissivity, and f_{SF} is the snow cover fraction.

2.3.2 Mathematical Description

2.3.2.1 Bare emissivity climatology

Land surface bare ground can be roughly classified into three types: bare soil, permanent ice & snow, and inland water. Since the emissivity of each type differs from others, the bare emissivity climatology was processed separately with the assistance of the surface type data. Soil covered with/without vegetation constitutes most of the land surface, whose emissivity is the key part of the climatology.

ASTER GED is a mean emissivity database developed by the National Aeronautics and Space Administration's (NASA) Jet Propulsion Laboratory (JPL), California Institute of Technology, from all available clear-sky ASTER data between 2000 and 2008. The version

3 provides a static emissivity of 5 ASTER TIR bands with an average band error of ~1%.This global gridded data was released in 1x1 degree tiles at ~100m and ~1km spatial resolution, respectively (Hulley et al. 2015). The 1km dataset was used to generate bare ground emissivity climatology by reversing equation (2-1):

$$\varepsilon_{AST,bare} = \frac{\varepsilon_{AST} - \varepsilon_{veg} f_{v,AST}}{1 - f_{v,AST}} \quad (2\text{-}3)$$

where ε_{AST} is the ASTER GED v3 emissivity, $\varepsilon_{AST,bare}$ and ε_{veg} is the ASTER bare and vegetation component emissivity, and $f_{v,AST}$ is the ASTER vegetation cover fraction.

In equation (2-3), ε_{veg} was originally the mean value from ASTER spectral library. However, very low values were found over dense vegetation in GED v3 data, in which pixels with FVC greater than 0.9 have the mean emissivities of 0.972, 0.971, 0.969, 0.974, and 0.974 for the 5 ASTER TIR bands, respectively. Compared with the spectral library value of 0.987, 0.983, 0.979, 0.981 and 0.983, the discrepancy could be up to 0.01, which is significant difference in emissivity. The overestimated ε_{veg} used in (2-3) may result in an underestimated bare ground emissivity. Therefore, a modification of equation (2-3) is made to use the vegetation component emissivity derived from product instead of that from spectral library. In addition, to address the difference between vegetation types, the vegetation component emissivity was surface type dependent. The result confirms this assumption, i.e. the needle leaf forest has highest emissivity while the savannah is the lowest. There is a difference of almost 0.01 between them.

The bare emissivity climatology derived from ASTER GED v3 covers ASTER 5 TIR bands, which are different from VIIRS and ABI split window bands (Figure 2-3). A linear conversion is constructed to get the channel emissivity ε_i

$$\varepsilon_i = c_0 + c_1\varepsilon_{10} + c_2\varepsilon_{11} + c_3\varepsilon_{12} + c_4\varepsilon_{13} + c_5\varepsilon_{14} \quad (2\text{-}4)$$

where, ε_{10} - ε_{14} are the five ASTER channel emissivities, and c0 - c5 are the coefficients determined by regression. Since this conversion is designed for the bare soil, a spectral set of soil, rocks and a few construction material including asphalt and concrete were selected from ASTER spectral library for the regression. Both the source and target channel emissivity were convoluted with their corresponding spectral response function.

The coefficients were summarized in Table 2-3. Considering the correlation between source and target channels, the 11μm channel was just calculated by ASTER B13 and B14. Although it's difficult to convert the emissivity of 12μm band due to little overlap with ASTER bands, the correlation with adjacent bands emissivity for a certain type is good enough to get an acceptable conversion. Previous studies have shown that 8 - 13.5μm spectral domain

could represent the broadband emissivity best, and the BBE could be modeled using ASTER narrow TIR bands (Cheng et al. 2013).

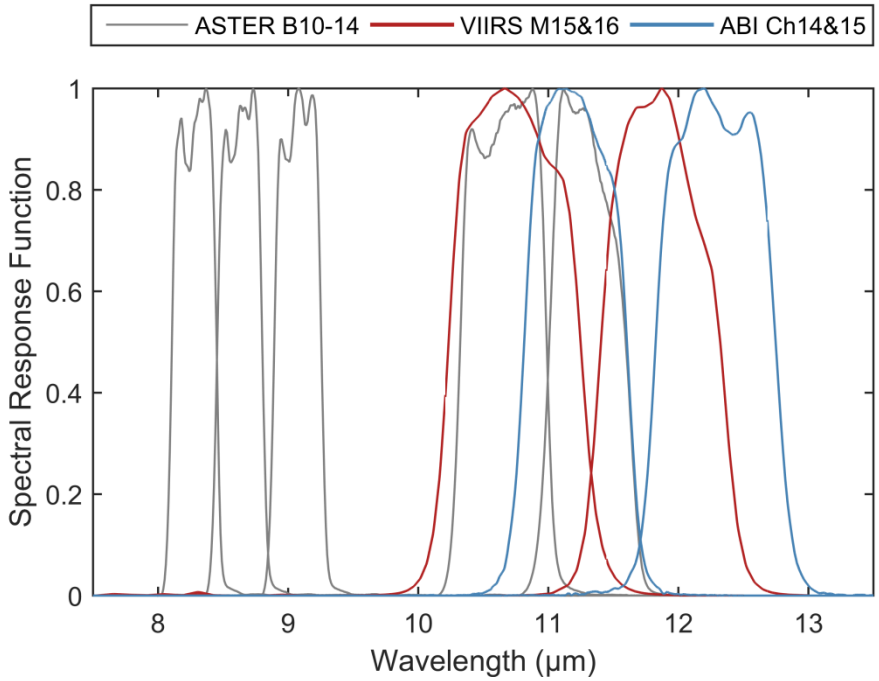

Figure 2-3 Spectral response functions of ASTER, VIIRS and ABI TIR bands

Table 2-3 Coefficients of the spectral conversion equation

	C0	C1	C2	C3	C4	C5	R2
VIIRS M15	-0.0117	---	---	---	0.8453	0.1661	0.9988
VIIRS M16	0.4099	-0.0006	0.0095	-0.0264	0.1048	0.4948	0.9250
ABI Ch14	-0.0256	---	---	---	0.1644	0.8228	0.9992
ABI Ch15	0.5125	0.0145	0.0042	0.0291	-0.0176	0.4520	0.9080
Broadband	0.1949	0.1075	0.0664	0.1233	0.3925	0.1111	0.9921

Permanent snow and ice occupies a large area at polar region, however, there are no ASTER GED data at Antarctic areas. Besides the permanently covered snow and ice at northern hemisphere have a much lower emissivity than the spectral library value. Current data also indicated snow and ice emissivity vary in types, *e.g.*, generally ice and coarse snow have lower emissivity than fine or fresh snow (Salisbury et al. 1994). An alternative emissivity product is required to map snow emissivity, rather than the mean library data. University of Wisconsin Global Infrared Land Surface Emissivity Database (UWIREMIS) database is derived from MODIS emissivity product could extend to high resolution emissivity spectra 3.6 and 14.3 microns and serves the need well. Using the same method for ASTER GED, UWIREMIS mean emissivities at 10 channels were generated from the monthly data between

2003 and 2014. A high spectral resolution algorithm was employed to generate finer resolution data, which was then convoluted to the emissivity of VIIRS, ABI SW bands and 8 - 13.5μm broadband. Compared with ASTER GED, corresponding channel emissivity derived from MODIS mean emissivity works better over the snow area as Figure 2-4 shows.

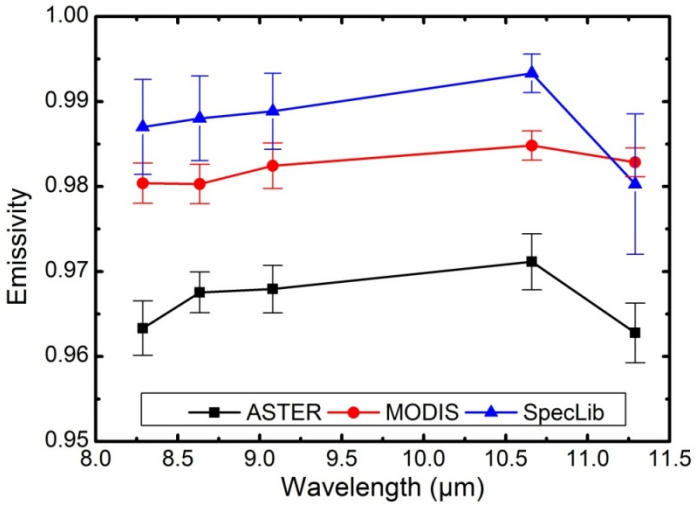

Figure 2-4 Snow/Ice emissivities of MODIS, ASTER GED, and spectral library at ASTER TIR channels

Based on the analysis above, climatology of the permanent snow and ice area is replaced by the mean value derived from UWIREMIS after re-sampling from 0.05 degree to 0.009 degree. Given the high homogeneity of snow area, this procedure will not introduce significant uncertainty.

For the third type, namely inland water is always regarded as black body for its high emissivity. ASTER emissivity product might not work very well at the surface with low-contrast spectral therefore the average value from spectral library was used according to the surface type data. Additionally, once the water gets frozen at high latitude area, the ice emissivity will be used instead, which is much lower than that of water.

It should be noted that there are nearly 1% pixels with either missing values or unreasonable values (larger than 1 or less than 0.6) in ASTER GED dataset due to cloud contamination, spatial coverage, or inversion issues. These were replaced by the mean value of adjacent available pixels with the same surface type. The effective radius was set as 2.5 degree. If there are no enough available pixels, a global mean value of that surface type will be used.

An example of the global gridded background emissivity climatology was shown in Figure 2-5.

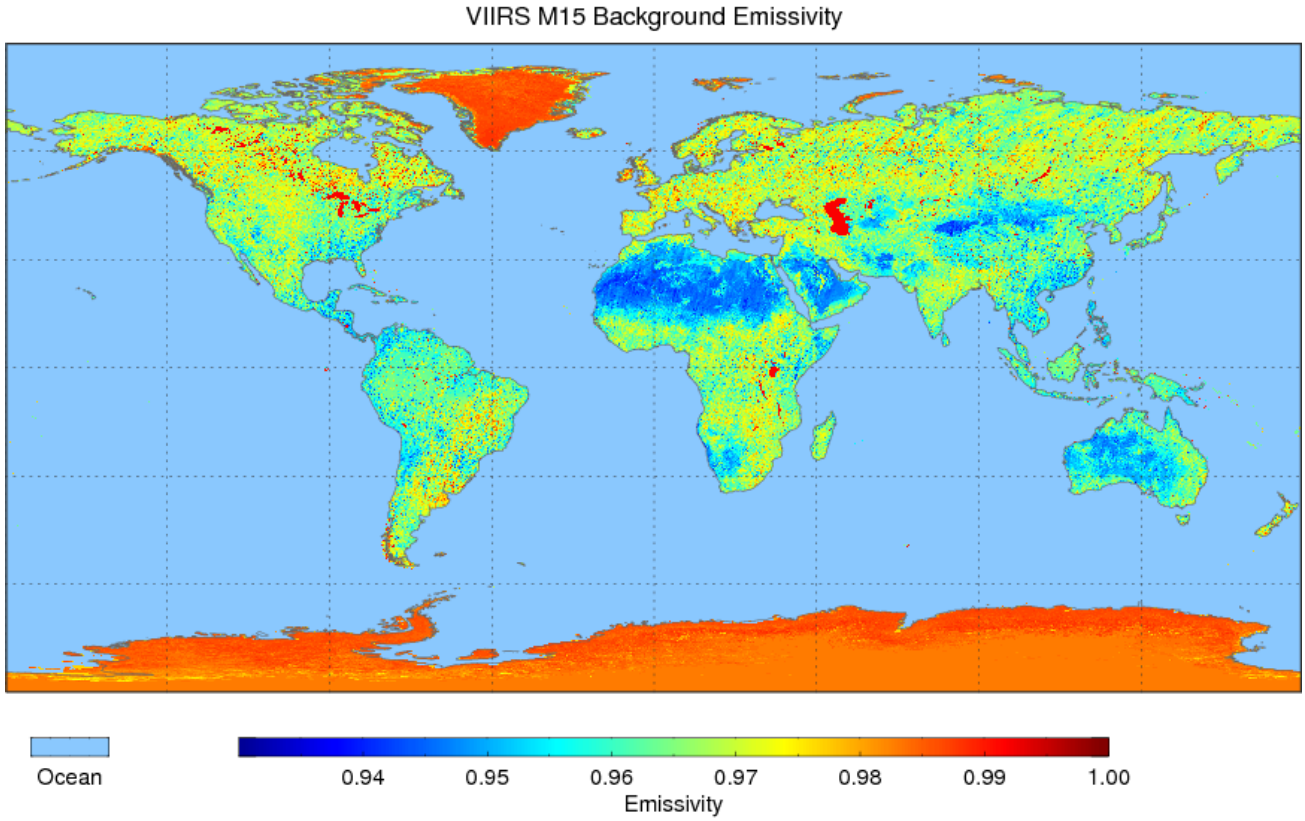

Figure 2-5 VIIRS M15 background emissivity

2.3.2.2 Dynamic emissivity

Based on the bare ground emissivity climatology, the real time vegetation fraction data was used to adjust the emissivity by equation (1), in which the climatology works as the soil component emissivity, while the vegetation one was assigned according to the spectral library. The cavity term is defined below

$$d\varepsilon_\lambda = 4\langle d\varepsilon_\lambda \rangle f(1-f) \tag{2-5}$$

where $\langle d\varepsilon_\lambda \rangle$ is the maximum cavity effect value, which is assumed to exist under nadir observation and can be simplified as

$$\langle d\varepsilon_\lambda \rangle = (1-\varepsilon_\lambda^{bare})\varepsilon_\lambda^{veg} F(1-f) \tag{2-6}$$

where, F is the shape factor in the "box model" depending on the vegetation height and separation.

Both the vegetation component emissivity and cavity term depend on surface type and will be estimated based on the IGBP database. The vegetation emissivity for each type is

assigned as (Trigo et al. 2008) configured library samples for SEVIRI. The detailed values for each surface type are shown in Table 2-4

Table 2-4 Mean vegetation emissivity and cavity term for each surface type

IGBP Class	M15	M16	Ch14	Ch15	BBE	F
1, 2	0.989	0.991	0.989	0.991	0.991	0.92
3, 4	0.974	0.973	0.973	0.974	0.977	0.92
5	0.981	0.982	0.981	0.983	0.984	0.92
6	0.981	0.982	0.981	0.983	0.984	0.65
7	0.981	0.982	0.981	0.983	0.984	0.14
8	0.967	0.968	0.967	0.970	0.973	0.65
9	0.965	0.967	0.965	0.969	0.971	0.38
10	0.982	0.988	0.985	0.989	0.983	0.08
12	0.982	0.988	0.985	0.989	0.983	0.38
13	0.982	0.985	0.983	0.986	0.983	0.08
14	0.975	0.978	0.977	0.979	0.979	0.79
16	0.965	0.967	0.965	0.969	0.971	0.05

To implement the vegetation adjustment, real-time vegetation fraction product is required. VIIRS GVF operational product developed by the NOAA/NESDIS Center for Satellite Applications and Research (STAR) is produced as a daily rolling weekly composite at 1 km resolution. This GVF product derived from enhanced vegetation index with uncertainty of ~12%. It should be noted that its data latency is one day after the 7-day compositing period. Such delay is considered acceptable for emissivity modeling, since the growth of plants is a relative slow process.

Currently, the 1-km VIIRS GVF is available for sub-region (130°E to 30°E, 90°N to 7.5°S) while the global one is at 4-km resolution. Therefore the global (4km) and regional (1km) weekly GVF data are used to generate a GVF composite intermediate output at 1km. The 1km global GVF will be produced in the near future to replace the degraded one.

To model the snow cover impact on emissivity, snow fraction product is used in the algorithm as described by (2-2). An operational VIIRS snow fraction product generated by NOAA/STAR is adopted here, which uses the reflectance of VIIRS visible band I1 (0.6-0.68μm) and applies a linear unmixing technique to empirically determine the snow portion (Romanov et al. 2003). In the operational processing, the gridded snow fraction of all granules data from the previous day is needed to make the composition, leading to one-day latency. Gaps in snow fraction product due to cloud, darkness at pole region or any other reason will be replaced by the latest available values. This might introduce uncertainty, especially when heavy snow fall event occurs. This processing might introduce some error especially when new snow fall

event occurs, a quality flag will be set to mark these pixels as non-instantaneous input for further diagnostics.

2.4 Algorithm Output

Output of the VIIRS LSE algorithm contains four data arrays: the LSE values and associated quality control flags, while ABI LSE with three, the quality flag works for both of them. (Tables 2-5 and 2-6).

Table 2-5 LSE algorithm output data description

Data Set	Variables	Description	Dimension
VIIRS LSE Product	emis_m15	Land surface emissivity value for each pixel of VIIRS M15	(xsize, ysize)[1]
	emis_m16	Land surface emissivity value for each pixel of VIIRS M16	(xsize, ysize)[1]
	emis_bbe	8- 13.5μ broadband emissivity value for each pixel	(xsize, ysize)[1]
	quality_flag	Quality control flags for each pixel	(xsize, ysize)[1]
ABI LSE Product	emis_ch14	Land surface emissivity value for each pixel of ABI Ch14	(xsize, ysize)[1]
	emis_ch15	Land surface emissivity value for each pixel of ABI Ch15	(xsize, ysize)[1]
	quality_flag	Quality control flags for each pixel	(xsize, ysize)[1]

1. xsize = 40000, ysize = 20000

Table 2-6 LSE product quality flag description

byte	bit	Flag	Source	description
1	0-1	Overall quality	Combined	00=Mean error [0, 0.005] 01=Mean error (0.005, 0.010] 10=Mean error (0.010, 0.015] 11=Mean error > 0.015
	2-3	Surface Type	Surface Type Land Sea Mask	00=Land, 01=Permanent snow/ice 10=Ocean, 11=Inland water
	4	GVF	VIIRS Gridded GVF	0 = Original 1km GVF 1 = Resampled 1km GVF from 4km data
	5	Snow	VIIRS Granule Snow Fraction	0 = instantaneous VIIRS snow fraction 1 = non instantaneous snow fraction
	6-7	For future use		

2.5 Performance Estimates

2.5.1 Test Data Description

Unit Tests have been conducted to verify whether LSE is correctly implemented in the NDE system. Dataset from three seasons (20170109, 20170409 and 20170709) with a wide range of vegetation and snow fraction have been selected for product verification. These datasets include the static input data designed for LSE algorithm, which have been introduced in section 2.2, such as background emissivity climatology, VIIRS annual surface type and the look-up tables. For these certain days, dynamic input data are prepared for test as follows:

- Daily rolling weekly GVF data Global 4km and North America regional 1km. s20170103_e20170109, s20170403_e20170409, s20170703_e20170709
- VIIRS snow fraction EDR: all granules of 20170109, 20170409 and 20170709
- Previous day (Day-1) global gridded gap free snow fraction: 20170108, 20170408 and 20170708

Eventually, daily LSE products of these days are produced, as Figure 2-6 shows.

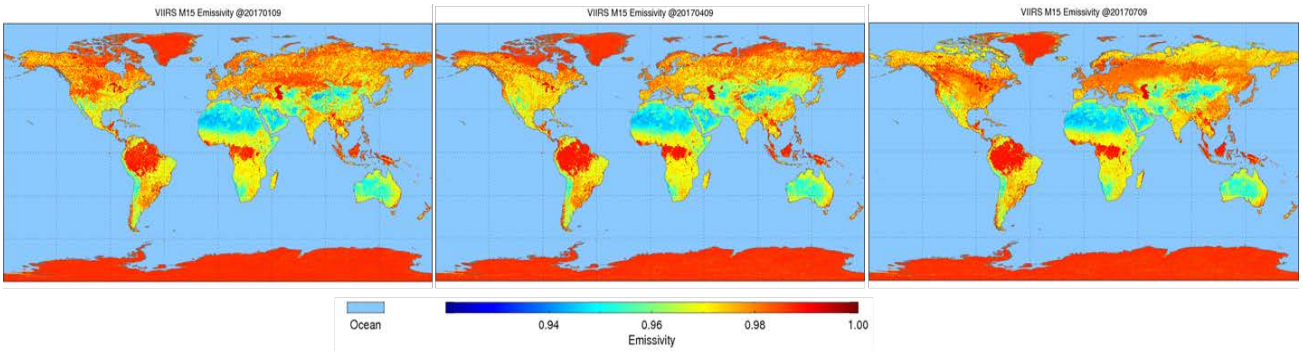

Figure 2-6LSE product verification dataset

Although the in-situ emissivity measurement is still a challenge and is very limited, it is the most effective and reliable dataset for algorithm validation. The primary ground emissivity dataset was collected in northwest China in 2012 under the context of Heihe Watershed Allied Telemetry Experimental Research (HiWATER). The corresponding satellite LSEs are produced corresponding to the ground observation time. Four barren sites measurements were obtained on July 10, 2012 and three observations at different growing stages (20120530, 20120615 and 20120624) were made over a vegetation site. Besides, performance of long time LST derived from LSE are also used to evaluate the product.

2.5.2 Sensor Effects

LSE product is generated based on VIIRS EDR as well as historical emissivity climatology rather than directly retrieved from sensor data record (SDR). Sensor effects such as its random noise, calibration error and geolocation uncertainty will indirectly impact LSE accuracy through the retrieval error of VIIRS GVF, snow fraction and surface type. More detailed information about the errors of these products can be found from the related algorithm theoretical basis documents, while their impact on LSE will be characterized in the following section.

2.5.3 Retrieval Errors

To quantify the uncertainty in the emissivity product, the theoretical emissivity error is calculated based on the error propagation theory. LSE retrieval error budget contains three types of uncertainty sources: the bare ground emissivity uncertainty, GVF error and VCM method uncertainty, snow fraction error and linear mixing uncertainty.

The bare ground climatology uncertainty largely depends on the quality of ASTER GED. ASTER GED is mean value of clear sky emissivity product retrieved using TES algorithm after an enhanced atmospheric correction named water vapor scaling method. The uncertainty has been quantified through the temperature and emissivity uncertainty simulator (Hulley et al. 2012), in which the band-dependent emissivity error is quantified as a function of the total column water for three surface types (bare, gray body and the transition). Besides, the emissivity conversion between ASTER and VIIRS/ABI channels will also introduce uncertainty, especially for the 12μm bands due to the less overlap with ASTER. All these uncertainties are assumed to be independent. The combined error could be calculated using (2-7).

$$\delta\varepsilon = \sqrt{\sum_{i=1}^{n}\left(\delta\varepsilon_i\right)^2} \tag{2-7}$$

For the dynamic emissivity, the errors of GVF and snow fraction contribute to the product uncertainty along with the climatology. The uncertainty of VCM could be described as (2-8)

$$\delta\varepsilon_{VCM} = f_v\delta\varepsilon_v + \left(1-f_v\right)\delta\varepsilon_g + 4f_v\left(1-f_v\right)\delta\left\langle d\varepsilon\right\rangle + \left[\varepsilon_v - \varepsilon_g + 4\left\langle d\varepsilon\right\rangle\left(1-2f_v\right)\right]\delta f_v \tag{2-8}$$

where, $\delta\varepsilon_g$ is the bare ground emissivity uncertainty mentioned above, $\delta\varepsilon_v$ is the vegetation emissivity uncertainty, using the standard deviation of the emissivity from the spectral library, δf_v is the GVF product error.

Similar to the GVF, the uncertainty brought during the snow effect calculation could be calculated as (2-9)

$$\delta\varepsilon = f_s\delta\varepsilon_{VCM} + (1 - f_s)\delta\varepsilon_s + (\varepsilon_s - \varepsilon_{VCM})\delta f_s \quad (2\text{-}9)$$

Where, $\delta\varepsilon_{VCM}$ is result of (2-8), and $\delta\varepsilon_s$ is snow emissivity uncertainty from the spectral library, and δf_s represents the snow fraction product uncertainty.

The mean emissivity errors of the split window channels are grouped into four bins: [0, 0.005], [0.005, 0.010], [0.010, 0.015] and 0.015 beyond. Figure 2-7 shows a case on 20170409, in which the emissivity uncertainty shows a global distribution of 1.17%, 75.91%, 22.88% and 0.04% for each category.

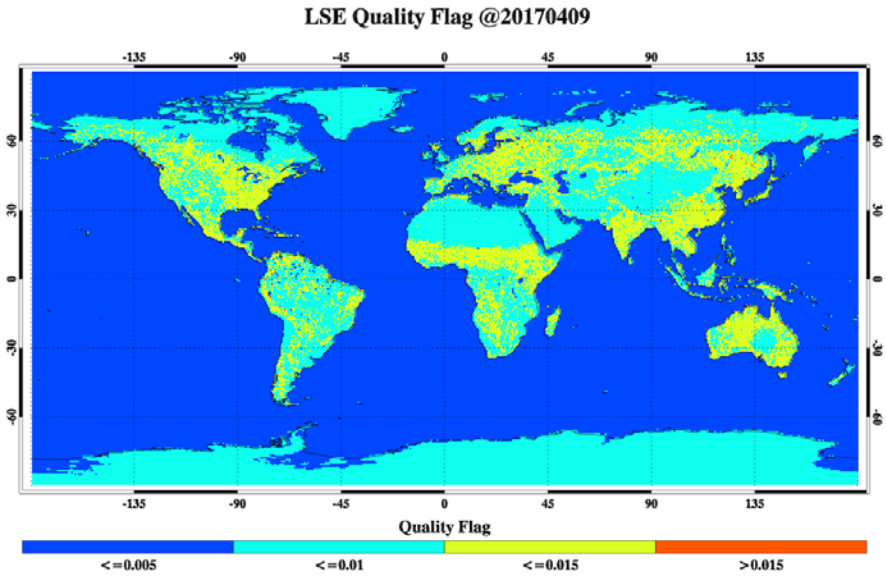

Figure 2-7 LSE overall quality on April 9, 2017

2.6 Practical Considerations

2.6.1 Numerical Computation Considerations

The LSE product is developed using a semi-empirical algorithm with basic mathematical routines, which are robust and computationally efficient. For storage consideration, LSE values are scaled to signed byte, with scale factor and offset defined in the attributes. Quality flags for each pixel value should be bit-flag definitions, to minimize data storage.

2.6.2 Programming and Procedural Considerations

The simplicity of the algorithms described in this document is translated into small amount of code using basic mathematical routines. Since the daily LSE data size is very large due to

its global coverage and high spatial resolution, it is partitioned to multiple segments with smaller data size.

2.6.3 Quality Assessment and Diagnostics

The LSE overall quality flags are designed according to the system requirement. And a couple of parameters and indicators are reported in the LSE product as retrieval diagnostic flags, for example, the GVF resolution and latency flag of snow fraction help to diagnose the data quality. The lists of quality flags as well as their detailed descriptions are given in section 2.4.
Statistical information is also included in the product, *e.g.*, the minimum and maximum value, each quality group percentage etc.

2.6.4 Exception Handling

The algorithm will handle exceptions by input/output data check and quality flags. LSE is designed as a gap-free global product. When generating the bare ground emissivity climatology, the missing value and pixel with poor quality will be replaced by the interpolated value.
If there is no GVF data available for certain day; the latest one will be used. Once the latency is longer than 15 days, the monthly GVF climatology will be employed instead. This climatology is the mean value of each month, generated using all the SNPP/VIIRS daily rolling weekly GVF from 2013 to 2017.
For the snow fraction, there are two types of input data: the VIIRS granule snow fraction and the previous gridded data used for the gap filling. If they do not exist, the latest available one will be used. Same as the GVF, the maximum latency is set to 15 days, the monthly snow fraction climatology will works as substitute once there is no data within 15 days. The snow climatology is generated using SNPP/VIIRS snow fraction from2014 to 2017.

2.7 Validation

2.7.1 LSE validation

A series of in situ emissivity measurements were carried out in northwest China in 2012 under the context of Heihe Watershed Allied Telemetry Experimental Research (HiWATER) (Li et al. 2013). Ground emissivity was collected at four barren sites for once and cropland areas at three different growing stages. Four large homogeneous sites located in the arid area were chosen for LSE evaluation. There are three typical surface types in this region

including the gobi site (GB), desert site (SSW) and two desert steppe sites (HZZ, JCHM), as Figure 2-8 shows.

The emissivity was acquired by an ABB BOMEM MR304 Fourier Transform Infrared Spectroscopy which is a high-precision instrument with a spectral resolution of up to 1cm^{-1} in 2-15 μm range. Under field conditions, the targets and downward sky radiance was measured using the MR304 and a diffuse golden plate and the emissivity was retrieved by the Iterative Spectrally Smooth Temperature and Emissivity Separation (ISSTES) algorithm, with an accuracy better than 0.01(Wang et al. 2015). The LSE data derived from the product was compared with the field measured emissivity spectra convolved with the spectral response function of VIIRS and ABI SW bands. The results indicate that LSE algorithm works well for these bare surfaces with pretty good agreement within 0.006 for narrow bands and 0.012 for broadband.

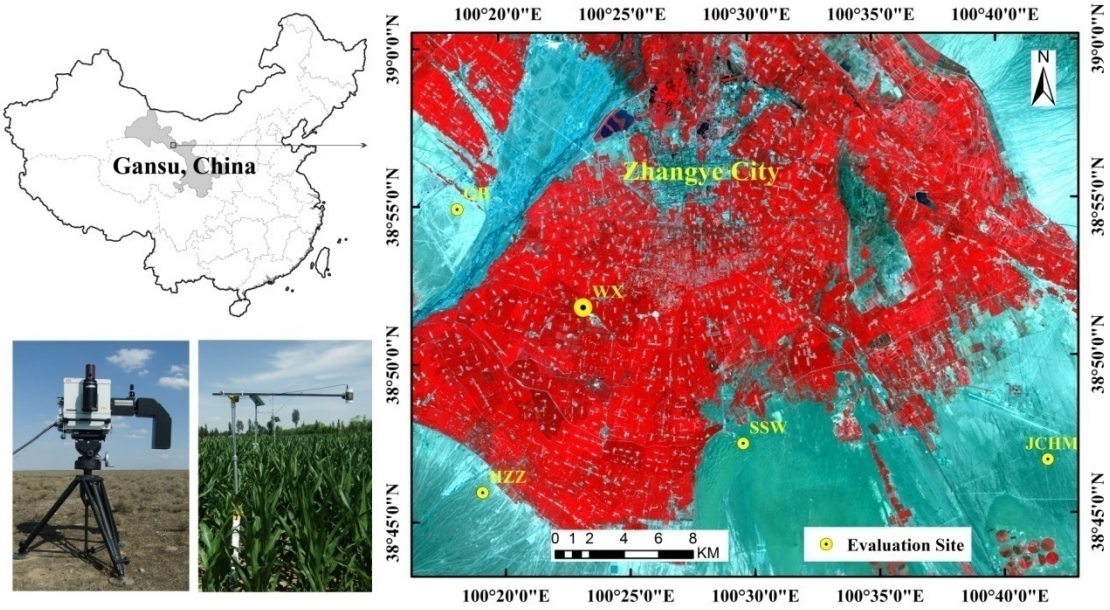

Figure 2-8 LSE in situ validation sites

To evaluate dynamic emissivity, a corn field (WX) located in the artificial oasis was selected to evaluate the vegetated area with various GVF. To facilitate the measurement over canopy, a more compact multichannel thermal infrared radiometer (CE312-2) with 5 narrow bands (8.25-8.60, 8.49-8.86, 8.95-9.34, 10.16-10.96, 10.86-11.71μm) and a broadband channel (8.01-13.34μm) was used. This radiometer has a field view of 10° and was mounted at least 1 meter above the top of canopy to collect the radiation from the mixed scenes. 5 narrow band emissivities along with LST were retrieved using ASTER TES algorithm; consequently,

the broadband emissivity could be determined using Planck function using the retrieved LST in TES. Since CE312-2 is a multichannel radiometer with similar channel as ASTER, it could not be directly compared with the VIIRS and ABI emissivity product. Considering that the product is derived from ASTER GED, an alternative approach to evaluate the dynamic emissivity is to produce emissivity of ASTER 5 TIR channels using current algorithm. The result shows LSE product works well at this site with a mean accuracy of ~0.007 for ASTER channels.

2.7.2 Evaluating LSE in LST retrieval

Currently, LSE field measurement is still a challenge. In situ measurements are still limited and long-term LSE monitoring using ground data is nearly impossible. LSE product is proposed primarily for LST retrieval, in which LSE accuracy will significantly impact the LST quality. What's more, there are long-term LST ground measurements available for evaluation, so LST retrieval accuracy could be regarded as an alternative criterion for LSE quality. To evaluate the LST accuracy, the temperature based method was adopted, which involves direct comparison with ground measurements performed at the thermally homogenous sites concurrent with the satellite overpass.

The SURFace RADiation budget observing network (SURFRAD) provides high quality long-term measurements of surface upwelling and downwelling long wave radiations along with other meteorological parameters (Augustine et al. 2000). There are seven sites available for the LST validation. Each station is equipped with a pyranometer on a 10 meter high tower with a field-of-view approximate70 m × 70 m. SURFRAD observations from February 2012 to July 2015 are used for validation of the VIIRS LST retrieval.

The spectral emissivity data has been applied to a variety of emissivity-explicit LST algorithms including the VIIRS enterprise LST algorithm. The derived LSTs have been evaluated against in situ measurements and show promising quality.

These validation activities mentioned above are preliminary results, more substantial algorithm and product validations are necessary.

3 ASSUMPTIONS AND LIMITATIONS

3.1 Performance Assumptions

The following assumptions have been made in the LSE algorithm development and quality evaluations.

- The basic assumption of VCM is that land surface pixels contain two components: bare ground and vegetation and emissivities of the two components do not change over time. Vegetation emissivity and 3-D structure are surface type dependent, thus each IGBP class has same vegetation emissivity and cavity correction factors.
- Weekly composited GVF data after noise filtering is available and vegetation fraction doesn't have dramatic change during one week.
- Permanent snow/ice emissivity is homogenous at 0.05×0.05 degree grids, thus degraded MODIS snow emissivity at 5km resolution will not introduce significant uncertainty. Since there is no data in the area under polar night, we assume snow fraction will not change during the darkness period.

Based on the assumptions mentioned above, LSE product has its limitations:

- Currently, the emissivity is designed for nadir view only without consideration of the angular effect of emissivity.
- GVF and snow fraction are the only two factors controlling the variation of emissivity. Soil moisture has not been taken into account in the current algorithm, which will result in a constant value for barren area with no vegetation and snow.
- Snow fraction data has at least one day latency, the pixels with new heavy snow fall might have larger uncertainty due to lack of instantaneous data.

3.2 Potential Improvements

Soil moisture has proved to have significant impact on emissivity. However, bare ground emissivity as a static value in LSE algorithm made great contribution at low GVF areas. While this is acceptable for arid areas with extremely low soil moisture, it might introduce large uncertainty at the sparse vegetation area with large soil moisture fluctuations. A potential improvement in the future will be soil moisture correction, which will improve the LSE quality over low GVF area.

For the validation part, ground measurements are still very limited, and more in-situ emissivity from different areas could be collected through international collaborations, which will highly support LSE product.

4 REFERENCES

Augustine, J. A., J. J. DeLuisi and C. N. Long (2000). "SURFRAD - A national surface radiation budget network for atmospheric research." Bulletin of the American Meteorological Society 81(10): 2341-2357.

Baldridge, A., S. Hook, C. Grove and G. Rivera (2009). "The ASTER spectral library version 2.0." Remote Sensing of Environment**113**(4): 711-715.

Becker, F. (1987). "The impact of spectral emissivity on the measurement of land surface temperature from a satellite." International Journal of Remote Sensing**8**(10): 1509-1522.

Borbas, E. A high spectral resolution global land surface infrared emissivity database.

Cao Changyong, Xiong Jack, Blonski Slawomir, Liu Quanhua, Uprety Sirish, Shao Xi, Bai Yan and Weng Fuzhong, “Suomi NPP VIIRS sensor data record verification, validation, and long-term performance monitoring”, Journal of Geophysical Research: Aemosphere, Vol. 118, 11,664–11,678, doi:10.1002/2013JD020418, 2013.

Caselles, E., E. Valor, F. Abad and V. Caselles (2012). "Automatic classification-based generation of thermal infrared land surface emissivity maps using AATSR data over Europe." Remote Sensing of Environment**124**: 321-333.

Caselles, V. and J. A. Sobrino (1989). "Determination of Frosts in Orange Groves from Noaa-9 Avhrr Data." Remote Sensing of Environment**29**(2): 135-146.

Cheng, J., S. L. Liang, Y. J. Yao and X. T. Zhang (2013). "Estimating the Optimal Broadband Emissivity Spectral Range for Calculating Surface Longwave Net Radiation." Ieee Geoscience and Remote Sensing Letters**10**(2): 401-405.

Dash, P., F. M. Göttsche, F. S. Olesen and H. Fischer (2002). "Land surface temperature and emissivity estimation from passive sensor data: Theory and practice-current trends." International Journal of Remote Sensing**23**(13): 2563-2594.

Gillespie, A., S. Rokugawa, T. Matsunaga, J. Cothern, S. Hook and A. Kahle (1998). "A temperature and emissivity separation algorithm for Advanced Spaceborne Thermal Emission and Reflection Radiometer(ASTER) images." Ieee Transactions on Geoscience and Remote Sensing**36**(4): 1113-1126.

Hulley, G. C., S. J. Hook, E. Abbott, N. Malakar, T. Islam and M. Abrams (2015). "The ASTER Global Emissivity Dataset (ASTER GED): Mapping Earth's emissivity at 100 meter spatial scale." Geophysical Research Letters**42**(19): 7966-7976.

Hulley, G. C., C. G. Hughes and S. J. Hook (2012). "Quantifying uncertainties in land surface temperature and emissivity retrievals from ASTER and MODIS thermal infrared data." Journal of Geophysical Research-Atmospheres**117**(D23).

Jiménez-Muñoz, J. C. (2003). "A generalized single-channel method for retrieving land surface temperature from remote sensing data." Journal of Geophysical Research**108**(D22).

Jin, M. and S. Liang (2006). "An improved land surface emissivity parameter for land surface models using global remote sensing observations." Journal of Climate**19**(12): 2867-2881.

Li, X., G. Cheng, S. Liu, Q. Xiao, M. Ma, R. Jin, T. Che, Q. Liu, W. Wang and Y. Qi (2013). "Heihe Watershed Allied Telemetry Experimental Research (HiWATER): Scientific Objectives and Experimental Design." Bulletin of the American Meteorological Society.

Li, Z.-L., B.-H. Tang, H. Wu, H. Ren, G. Yan, Z. Wan, I. F. Trigo and J. A. Sobrino (2013). "Satellite-derived land surface temperature: Current status and perspectives." Remote Sensing of Environment**131**: 14-37.

Liu, Y. L., Y. Y. Yu, D. L. Sun, D. Tarpley and L. Fang (2013). "Effect of Different MODIS Emissivity Products on Land-Surface Temperature Retrieval From GOES Series." Ieee Geoscience and Remote Sensing Letters**10**(3): 510-514.

Peres, L. F. and C. C. DaCamara (2005). "Emissivity maps to retrieve land-surface temperature from MSG/SEVIRI." Ieee Transactions on Geoscience and Remote Sensing**43**(8): 1834-1844.

Peres, L. F., R. Libonati and C. C. DaCamara (2014). "Land-Surface Emissivity Retrieval in MSG-SEVIRI TIR Channels Using MODIS Data." Ieee Transactions on Geoscience and Remote Sensing**52**(9): 5587-5600.

Qin, Z. H., G. Dall'Olmo, A. Karnieli and P. Berliner (2001). "Derivation of split window algorithm and its sensitivity analysis for retrieving land surface temperature from NOAA-advanced very high resolution radiometer data." Journal of Geophysical Research-Atmospheres**106**(D19): 22655-22670.

Romanov, P., D. Tarpley, G. Gutman and T. Carroll (2003). "Mapping and monitoring of the snow cover fraction over North America." Journal of Geophysical Research: Atmospheres**108**(D16).

Salisbury, J. W., D. M. Daria and A. Wald (1994). "Measurements of Thermal Infrared Spectral Reflectance of Frost, Snow, and Ice." Journal of Geophysical Research-Solid Earth 99(B12): 24235-24240.

Seemann, S. W., E. E. Borbas, R. O. Knuteson, G. R. Stephenson and H. L. Huang (2008). "Development of a global infrared land surface emissivity database for application to clear sky sounding retrievals from multispectral satellite radiance measurements." Journal of Applied Meteorology and Climatology**47**(1): 108-123.

Schmit, T. J., W. Paul Menzel , J. Gurka , M. Gunshor, “The ABI on GOES-R, 3rd Annual Symposium Future National Operational Environmental Satellite Systems”, San Antonio, January 16, 2007.

Snyder, W. C., Z. Wan, Y. Zhang and Y. Z. Feng (1998). "Classification-based emissivity for land surface temperature measurement from space." International Journal of Remote Sensing**19**(14): 2753-2774.

Trigo, I. F., L. F. Peres, C. C. DaCarnara and S. C. Freitas (2008). "Thermal land surface emissivity retrieved from SEVIRI/meteosat." Ieee Transactions on Geoscience and Remote Sensing**46**(2): 307-315.

Valor, E. and V. Caselles (1996). "Mapping land surface emissivity from NDVI: Application to European, African, and South American areas." Remote Sensing of Environment**57**(3): 167-184.

Vogel, R. L., Q. H. Liu, Y. Han and F. Z. Weng (2011). "Evaluating a satellite-derived global infrared land surface emissivity data set for use in radiative transfer modeling." Journal of Geophysical Research-Atmospheres**116**.

Wan, Z. and Z. L. Li (1997). "A physics-based algorithm for retrieving land-surface emissivity and temperature from EOS/MODIS data." Geoscience and Remote Sensing, IEEE Transactions on**35**(4): 980-996.

Wan, Z. M. and J. Dozier (1996). "A generalized split-window algorithm for retrieving land-surface temperature from space." Ieee Transactions on Geoscience and Remote Sensing**34**(4): 892-905.

Wang, H., Q. Xiao, H. Li, Y. Du and Q. Liu (2015). "Investigating the Impact of Soil Moisture on Thermal Infrared Emissivity Using ASTER Data." Geoscience and Remote Sensing Letters, IEEE 12(2): 294-298.

Yu, Y., J. L. Privette and A. C. Pinheiro (2008). "Evaluation of split-window land surface temperature algorithms for generating climate data records." Ieee Transactions on Geoscience and Remote Sensing 46(1): 179-192.

Yu, Y. Y., J. L. Privette and A. C. Pinheiro (2005). "Analysis of the NPOESS VIIRS land surface temperature algorithm using MODIS data." Ieee Transactions on Geoscience and Remote Sensing 43(10): 2340-2350.

Yu, Y. Y., D. Tarpley, J. L. Privette, M. D. Goldberg, M. K. R. V. Raja, K. Y. Vinnikov and H. Xu (2009). "Developing Algorithm for Operational GOES-R Land Surface Temperature Product." Ieee Transactions on Geoscience and Remote Sensing**47**(3): 936-951.

END OF DOCUMENT